Three-dimensional structure of multicomponent $(Na_2O)_{0.35}[(P_2O_5)_{1-x}(B_2O_3)_x]_{0.65}$ glasses by high-energy x-ray diffraction and constrained reverse Monte Carlo simulations

2011 J. Phys.: Condens. Matter 23 035403

(http://iopscience.iop.org/0953-8984/23/3/035403)

J. Phys.: Condens. Matter **23** (2011) 035403 (10pp) doi:10.1088/0953-8984/23/3/035403

Three-dimensional structure of multicomponent $(Na_2O)_{0.35}[(P_2O_5)_{1-x}(B_2O_3)_x]_{0.65}$ glasses by high-energy x-ray diffraction and constrained reverse Monte Carlo simulations

Sébastien Le Roux[1,2], Steve Martin[3], Randi Christensen[3], Yang Ren[4] and Valeri Petkov[1]

[1] Department of Physics, 230 Dow Science, Central Michigan University, Mount Pleasant, MI 48859, USA
[2] Institut de Physique et Chimie des Matériaux de Strasbourg, F-67034 Strasbourg, Cedex 2, France
[3] Department of Materials Science and Engineering, Iowa State University, Ames, IA 50011, USA
[4] Advanced Photon Source, Argonne National Laboratory, Argonne, IL 60439, USA

E-mail: petkov@phy.cmich.edu

Received 21 October 2010, in final form 6 December 2010
Published 5 January 2011
Online at stacks.iop.org/JPhysCM/23/035403

Abstract

Experimental structure functions for $(Na_2O)_{0.35}[(P_2O_5)_{1-x}(B_2O_3)_x]_{0.65}$ glasses, where $x = 0.0$, 0.2, 0.4, 0.6, 0.8 and 1.0, have been measured by high-energy x-ray diffraction up to wavevectors of 28 $Å^{-1}$ to obtain atomic pair distribution functions with high real space resolution. The experimental diffraction data have been used to guide constrained reverse Monte Carlo simulations of the three-dimensional structure of the glasses. The resulting models show that the glasses exhibit a very complex atomic-scale structure that evolves from an assembly of chains of corner shared $P(O)_4$ tetrahedra for $x = 0$ to a network of $B(O)_4$ tetrahedra and planar $B(O)_3$ units for $x = 1$. In the glasses of intermediate composition (i.e. $0 < x < 1$), P, B and oxygen atoms sit on the vertices of $P(O)_4$, $B(O)_4$ and $B(O)_3$ units mixed in various proportions. Sodium atoms are found to fill up the cavities in between the P/B–oxygen units in a more or less random manner. The new data can provide a firm structural basis for an explanation of the mixed glass former effect where a nonlinear behavior of Na ion conductivity is observed in the $(Na_2O)_{0.35}[(P_2O_5)_{1-x}(B_2O_3)_x]_{0.65}$ glass system.

(Some figures in this article are in colour only in the electronic version)

1. Introduction

Sodium borophosphate glasses of the $(Na_2O)_y[(P_2O_5)_{1-x}(B_2O_3)_x]_{1-y}$ family are being extensively studied because of their fast ion conducting properties [1, 2]. It has been found that the conductivity of Na ions passes through a maximum when x, the ratio of glass network formers P and B, is varied between zero and one. This phenomenon has been observed in other glass systems [3] and has been called the mixed glass former effect (MGFE). This effect is believed to have a structural origin, yet a precise understanding of it is still lacking because of the structural complexity of the multicomponent glasses that exhibit it. The problem has been investigated by spectroscopic techniques such as IR, Raman [3]

and NMR [1, 2] that are sensitive to the type of structural units present in glasses. Recently we have begun to examine the structural origin of the MGFE using a combination of high-energy x-ray diffraction (XRD) and constrained reverse Monte Carlo (RMC) that are capable of building three-dimensional (3D) structure models and so yield a more detailed description of the atomic-scale glass structure. The quaternary system we studied, $(Li_2S)_{0.5}[(GeS_2)_{1-x}(GeO_2)_x]_{0.5}$, was composed of tetrahedral type $Ge(O)_4$ and $Ge(S)_4$ units across its whole compositional range [4]. Here, we apply the same approach to a much more complex, from a structural point of view, system, namely $(Na_2O)_{0.35}[(P_2O_5)_{1-x}(B_2O_3)_x]_{0.65}$, in which multiple structural units co-exist. It is the expectation that the new structural information we obtain will allow a better understanding of MGFE.

2. Experimental details

2.1. Sample preparation

Glasses of composition $(Na_2O)_{0.35}[(P_2O_5)_{1-x}(B_2O_3)_x]_{0.65}$, $0 \leqslant x \leqslant 1$, were prepared in platinum crucibles from the following starting materials: sodium carbonate Na_2CO_3 (Fisher Scientific); diammonium hydrogen phosphate $(NH_4)_2HPO_3$ (Fisher Scientific); and boric acid H_3BO_3 (Fisher Scientific). The starting materials were decomposed at 1000 °C for 0.5–1.5 h in air. After decomposition was complete, the melt was cooled to room temperature and transferred to a N_2 glove box where it was remelted at 900 °C for 10 min. Samples were quenched on brass plates at room temperature or in heated brass molds. Samples made in brass molds were annealed at 40 °C below T_g. All samples were prepared and stored in the N_2 glove box because of their hydroscopic nature. The glass density was determined using the Archimedes method with mineral oil (Fisher Scientific; $\rho_{oil} = 0.848$ g cm^{-3}).

2.2. High-energy x-ray diffraction experiments

X-ray diffraction experiments were carried out at the beam line 11IDC at the Advanced Photon Source using x-rays with energy of 115.232 keV ($k = 0.1076$ Å) and a large area (mar345) detector. Synchrotron radiation x-rays were used for two reasons. Firstly, the higher flux of synchrotron radiation x-rays makes it possible to measure the rather diffuse diffraction patterns of glasses with a very good statistical accuracy [5]. Secondly, the higher energy of synchrotron radiation x-rays makes it possible to reach higher wavevectors, Q, resulting in atomic distribution functions with very good real space resolution [6]. Glasses were sealed in thin walled quartz capillaries and measured at room temperature. Up to ten exposures were taken for each of the samples, and each exposure lasted 10 min. The experimental XRD data were reduced to Faber–Ziman type structure functions, $S(Q)$, defined as follows:

$$S(Q) = 1 + \left[I^{\text{coh.}}(Q) - \sum c_i |f_i(Q)|^2 \right] \Big/ \left| \sum c_i f_i(Q) \right|^2, \quad (1)$$

where c_i and f_i are the atomic concentration and scattering factor, respectively, for the atomic species of type i (here i = Na, P, O and B), Q is the wavevector and $I^{\text{coh}}(Q)$ the coherent component of the total diffracted intensities [6, 7]. The experimental $S(Q)$ data are shown in figure 1 up to the maximum wavevector of 28 Å^{-1} reached in the present experiments. Experimental atomic radial distribution functions (RDFs) $g(r) = \rho(r)/\rho_o$, where $\rho(r)$ and ρ_o are the local and average atomic number density and r is the radial distance, were obtained by a Fourier transformation [7] of the experimental structure functions using equations (2):

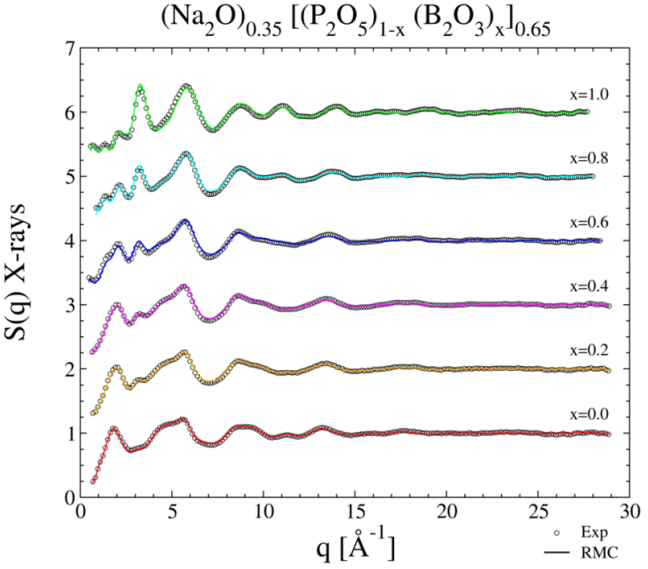

Figure 1. Experimental (symbols) and model (line) total x-rays structure functions for $(Na_2O)_{0.35}[(P_2O_5)_{1-x}(B_2O_3)_x]_{0.65}$ glasses with $x = 0.0$, 0.2, 0.4, 0.6, 0.8 and 1.0. The model data have been computed by constrained RMC simulations as described in the text. The goodness-of-fit factor is less than 5% for all simulations in the plot.

$$g(r) = 1 + \frac{1}{2\pi^2 \rho_o r} \int_{Q=o}^{Q_{\max}} Q[S(Q) - 1] \sin(Qr)\, \mathrm{d}Q. \quad (2)$$

These are shown in figure 2. The extraction of $I^{\text{coh}}(Q)$ from the raw diffraction intensities, the computation of $S(Q)$s and the derivation of the experimental $g(r)$s was done with the help of the program RAD [8]. Note that an atomic RDF obtained by a single diffraction experiment is a weighted sum of the contributions of all atomic pair correlations in the glass system under study, which are $n(n+1)/2$ in number for an n-component system. The weights [6, 7] of all atomic pair correlations in $(Na_2O)_{0.35}[(P_2O_5)_{1-x}(B_2O_3)_x]_{0.65}$ glasses, $0 \leqslant x \leqslant 1$, are listed in table 1. As can be seen in the table the individual contributions of Na, P, B and oxygen atoms to the experimental diffraction data come from like (e.g. Na–Na) and unlike (e.g. Na–P/B and Na–O) atomic pair correlations. The data in the table show that the combined contributions of Na, P, B and oxygen-involving atomic correlations are significant and comparable to each other (see table 1). For example, the combined contribution of Na-involving atomic correlations (i.e. the combined contribution of Na–Na, Na–P/B and Na–O correlations) ranges from 26% to 41% in the glasses with $x = 0$ and $x = 1.0$, respectively. Therefore, although the

Table 1. Weighting factors of the partial interatomic correlations in $(Na_2O)_{0.35}[(P_2O_5)_{1-x}(B_2O_3)_x]_{0.65}$ glasses. The sum of the weighting factors for a given glass composition, x, is one.

x	Na–Na	Na–P	Na–B	Na–O	P–P	P–B	P–O	B–B	B–O	O–O
0.0	0.019	0.096	0	0.14	0.12	0	0.358	0	0	0.264
0.2	0.022	0.091	∼0.01	0.15	0.092	0.015	0.316	∼0.01	0.026	0.270
0.4	0.027	0.082	0.018	0.174	0.063	0.028	0.265	∼0.01	0.058	0.279
0.6	0.034	0.068	0.034	0.197	0.035	0.035	0.199	∼0.01	0.099	0.289
0.8	0.042	0.043	0.058	0.226	0.011	0.03	0.115	0.02	0.153	0.301
1.0	0.056	0	0.094	0.266	0	0	0	0.04	0.225	0.319

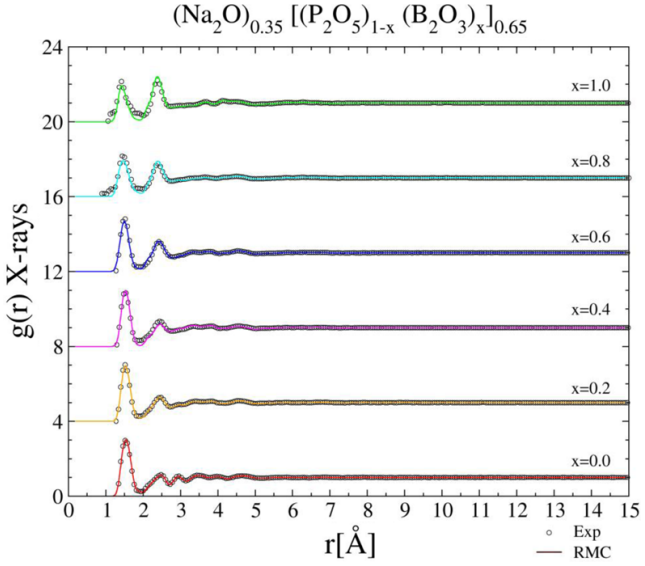

Figure 2. Experimental (symbols) and model (line) total x-ray radial distribution functions for $(Na_2O)_{0.35}[(P_2O_5)_{1-x}(B_2O_3)_x]_{0.65}$ glasses with $x = 0.0$, 0.2, 0.4, 0.6, 0.8 and 1.0. The model data have been computed by constrained RMC simulations as described in the text. The goodness-of-fit factor is less than 5% for all simulations in the plot.

glass modifier Na atoms do not participate in well defined structural units, and hence may not be associated with well defined features in the experimental RDF data, the latter is still sensitive to the former. The situation is similar, if not better, with P/B and oxygen-involving atomic correlations which not only make a significant contribution to the diffraction data (see the respective weighting factors in table 1) but, as discussed below, show up as well defined and thus easier to recognize RDF features.

2.3. Results

The atomic RDF is a continuous function that peaks at real space distances where distinct atomic pairs occur. It is a quantity defined in absolute units (see equations (1) and (2)) and so the area under the RDF peaks is directly proportional to the number of atomic pairs at those distances. This property of atomic RDFs makes them an experimental quantity that is very well suited for testing and refining of structure models. As can be seen in figure 2, the experimental RDFs for $(Na_2O)_{0.35}[(P_2O_5)_{1-x}(B_2O_3)_x]_{0.65}$ glasses show no peaks at distances longer than 10 Å, a behavior typical for glasses which, as a rule, lack long-range atomic ordering. At the same time, the experimental RDFs show very well defined peaks at small r distances indicating that all of the glasses studied have a very well defined short-range atomic order. In particular, the RDF for the glass with $x = 0$ has its first peak positioned at 1.52(2) Å which is the typical interatomic distance between the first neighbor P and O atoms sitting on the vertices of $P(O)_4$ tetrahedra, indicating the presence of such units in this glass. The result is consistent with previous NMR [1] and diffraction studies [9] of glasses of similar chemical composition.

Upon addition of boron, the short-range order in the glasses is seen to change substantially. The first RDF peak broadens and shifts to lower r values, reaching a position of 1.40(2) Å for the glass with $x = 1.0$. The second RDF peak increases in intensity and also gradually shifts to lower r values. For the glasses with $x = 1.0$ it is positioned at 2.36(2) Å. Interatomic B–O distances in the range of 1.35–1.55 Å and O–O distances in the range of 2.3–2.5 Å are found in trigonal $B(O)_3$ and tetrahedral $B(O)_4$ boron–oxygen units in sodium-borate glasses [10], indicating that the glass with $x = 1.0$ contains such units. On the basis of these experimental observations, it is plausible to assume that the glasses with $x = 0.2$, 0.4, 0.6 and 0.8 comprise $P(O)_4$, $B(O)_4$ and/or $B(O)_3$ units mixed in various proportions. The exact proportions of those units and the way they couple together into a structure lacking a long-range order were revealed by building and analyzing 3D structure models, as shown below.

An analysis of the experimental XRD data shows that not only the short, but the immediate-range order in these glasses also changes very substantially with the boron content. The latter changes are clearly demonstrated by the behavior of the low-Q part of the experimental $S(Q)$ data (see figure 1). In particular, the first sharp diffraction peak shifts its position from 1.84(1) $Å^{-1}$ with $(Na_2O)_{0.35}(P_2O_5)_{0.65}$ glass to 2.05(1) $Å^{-1}$ with $(Na_2O)_{0.35}(B_2O_3)_{0.65}$ glass; also, a new diffraction feature positioned at approximately 1.30 $Å^{-1}$ is seen to appear in the $S(Q)$ for the glasses of higher boron content (see figure 1). More details of the evolution of the short- and medium-range atomic order in the glasses studied here were revealed by constrained reverse Monte Carlo (RMC) simulations. The simulations were guided (i) by the experimental $g(r)$ and $S(Q)$ XRD data which, as discussed above, are sensitive to the interatomic correlations involving both the glass structure former (P/B) and glass structure modifier (Na) atoms, and (ii) by stringent structure-related constraints (e.g. see tables 2 and 3). The latter are very necessary in our case since a single diffraction data set alone may not be enough to precisely guide the structure modeling of

Table 2. Model box sizes, atomic model and experimental mass densities [18] used in the RMC simulations.

	$(Na_2O)_{0.35}[(P_2O_5)_{1-x}(B_2O_3)_x]_{0.65}$ glass					
	x					
	0.0	0.2	0.4	0.6	0.8	1.0
Model box edge (Å)	43.3602	42.6122	42.2581	42.3058	42.0395	40.7686
ρ_o (atoms Å^{-3})	0.071 190	0.077 208	0.081 670	0.082 939	0.087 715	0.091 999
ρ_o (g cm^{-3}) [18]	2.410	2.510	2.540	2.450	2.430	2.380

Table 3. Distances of closest interatomic approach (also known as 'cut-off' lengths) used in the RMC simulations.

Atomic pair	Cut-off length (Å)
Na–Na	2.40
Na–B	2.50
Na–P	2.50
Na–O	2.10
B–B	2.30
B–P	2.50
B–O	1.30
P–P	2.40
P–O	1.40
O–O	2.10

complex disordered systems. Using a combination of data from several experimental techniques such as x-ray and neutron scattering, NMR, Raman, IR spectroscopy and others would be the best way to go, when possible.

3. Modeling

Structural modeling was done by constrained RMC simulations that are capable of building large-size, and so statistically representative, atomic configurations subject to plausible chemical and physical constraints such as precise chemical composition, density, interatomic distances, bond angles and first coordination numbers. Each model configuration is positioned inside a simulation box subjected to periodic boundary conditions and refined against experimental, structure-sensitive data such as $S(Q)$ and $g(r)$. The refinement is done by varying the coordinates of the atoms from the model atomic configuration in a random manner so as to obtain the best possible agreement between the experimental and model computed $S(Q)$ and $g(r)$ within the imposed structural constraints [11, 12]. The simulations presented here were done with the help of the computer program RMC++ [13]. Note that although they are statistical in nature and so not a unique representation of the atomic arrangement, RMC-built models are well recognized and widely used as a tool for achieving a better understanding of the glass structure and properties related to it [11, 12].

At first, structural models for the end members (i.e. $x = 0.0$ and 1.0) of the $(Na_2O)_{0.35}$ $[(P_2O_5)_{1-x}(B_2O_3)_x]_{0.65}$ series of glasses were constructed as described below.

3.1. Modeling the structure of $(Na_2O)_{0.35}(P_2O_5)_{0.65}$ glass

The structure of $NaPO_3$ crystal [14] was used to build a starting model atomic configuration, since the RDF for $NaPO_3$ crystal showed many similarities with the experimental RDF for $(Na_2O)_{0.35}(P_2O_5)_{0.65}$ glass, indicating that the local atomic structure of that crystal and the glass are similar. Using crystallographic information, when available, can be very fruitful in structural studies of glasses, as discussed in [15]. Furthermore, it has been shown [16, 17] that the choice of the initial atomic configuration, even when it is of a crystalline type, can have a negligible effect on the results of RMC simulations when the latter are done with care. The stoichiometry of $(Na_2O)_{0.35}(P_2O_5)_{0.65}$ glass, however, is somewhat different from that of $NaPO_3$ crystal. To achieve the right stoichiometry we deleted an appropriate number of Na and O atoms from the crystal-based model, taking special care not to create under-coordinated P atoms. In other words, we ensured that already in the initial model configuration the greatest majority of P and O atoms sit on the vertices of $P(O)_4$ units as suggested by the preliminary analysis of the experimental RDF data. The model thus obtained consisted of 727 Na, 1350 P and 3737 O atoms filling the space with a density that is very close to the experimental one (see table 2). It was refined against the experimental XRD data observing appropriate minimum atomic approach distances listed in table 3.

3.2. Modeling of $(Na_2O)_{0.35}(B_2O_3)_{0.65}$ glass

To create the initial model configuration we used literature data [19] for the structure of sodium diborate $Na_2O \cdot (B_2O_3)_2$ crystal since, again, a model RDF for this crystal showed many similarities with the experimental RDF data for this sodium-borate glass. The stoichiometry of the model was adjusted to that of $(Na_2O)_{0.35}(B_2O_3)_{0.65}$ glass, taking special care that all boron atoms are three or four-fold coordinated with oxygen atoms, as suggested by the experimental RDF data. The model consisted of 500 Na, 921 B and 1696 O atoms filling up the space with a density close to the experimental one (see table 2). It was refined against the experimental XRD data observing appropriate minimum atomic approach distances listed in table 3.

3.3. Modeling of $(Na_2O)_{0.35}[(P_2O_5)_{1-x}(B_2O_3)_x]_{0.65}$ with $0 < x < 1$

The final atomic configuration of the $(Na_2O)_{0.35}(P_2O_5)_{0.65}$ glass model was used as an initial one for the $x = 0.2$ glass model. The correct stoichiometry was achieved by substituting some P atoms for B atoms, taking care that all B atoms are three- or four-fold coordinated by O atoms. Careful building and adjusting of initial model atomic configurations is found useful, and so is practiced not only in RMC but in

Table 4. Relative abundance (in %) of P-based units in $(Na_2O)_{0.35}[(P_2O_5)_{1-x}(B_2O_3)_x]_{0.65}$ glasses given in terms of $P^{(n)}$ and the related but more local-structure specific $P^{(n)}_{mB}$ polyhedra, where n = number of bridging oxygens and $mB \preceq n$ = number of boron atom neighbors[5] . Note that the total number of $P^{(n)}$ units (bold) in each of the glasses is normalized to 100%. The same normalization applies to the $P^{(n)}_{mB}$ units (italic).

	x				
	0.0	0.2	0.4	0.6	0.8
$P^{(1)}$	**6.9**	**3.1**		**3.4**	**3.5**
$P^{(1)}_{0B}$	*6.9*	*3.1*			
$P^{(1)}_{1B}$				3.4	3.5
$P^{(2)}$	**68.6**	**53.6**	**39.5**	**18.7**	**29.0**
$P^{(2)}_{0B}$	*68.6*	*32.1*	*14.5*	*2.5*	
$P^{(2)}_{1B}$		*19.3*	*18.2*	*8.4*	*2.7*
$P^{(2)}_{2B}$		*2.2*	*6.8*	*7.8*	*26.3*
$P^{(3)}$	**15.8**	**27.9**	**35.6**	**30.1**	**41.2**
$P^{(3)}_{0B}$	*15.8*	*9.3*	*3.9*		
$P^{(3)}_{1B}$		*10.2*	*11.2*	*7.1*	
$P^{(3)}_{2B}$		*6.3*	*13.7*	*12.8*	*4.9*
$P^{(3)}_{3B}$		*2.1*	*6.8*	*10.2*	*36.3*
$P^{(4)}$	**8.7**	**15.4**	**24.9**	**47.8**	**26.3**
$P^{(4)}_{0B}$	*8.7*	*5.1*	*2.2*	*2.4*	
$P^{(4)}_{1B}$		*3.9*	*3.8*	*8.7*	
$P^{(4)}_{2B}$		*4.9*	*7.5*	*15.7*	*2.7*
$P^{(4)}_{3B}$		*1.5*	*7.8*	*13.8*	*8.7*
$P^{(4)}_{4B}$			*3.6*	*7.2*	*14.9*

molecular dynamics (MD) studies on complex materials as well [20]. The model consisted of 783 Na, 1163 P, 293 B and 3737 O atoms and the density shown in table 2. The model was refined against the experimental XRD data observing the minimum atom approach distances shown in table 3. The final configuration for the $x = 0.2$ glass model was used to prepare the initial model for $x = 0.4$ glass in the manner described above. That model ended with 849 Na, 946 P, 631 B and 3737 O atoms and the density shown in table 2.

In a similar way, the final configuration of the $(Na_2O)_{0.35}(B_2O_3)_{0.65}$ glass model was used to prepare the initial configuration for the $x = 0.8$ glass model. Here some B atoms were replaced by P atoms and an appropriate number of P atoms were added taking care that all P atoms are four-fold coordinated by oxygen atoms. That model consisted of 1000 Na, 369 P, 1473 B and 3675 O atoms and the density reported in table 2. It was then refined against the experimental XRD data observing the minimum interatomic approach distances

[5] Note, the relative abundances of structure units shown in tables 4–7 are derived from models that are (i) refined against experimental data having a few per cent of unavoidable experimental error in it and (ii) large but yet limited in size. Therefore, the abundances, just like the respective structure models, should be looked at as statistical quantities subject to statistical fluctuations/error and not as unique analytical solutions. The error/statistical fluctuations in the abundances may not be less than the error in the experimental data used to guide the structure simulations, i.e. it is of the order of a few per cent.

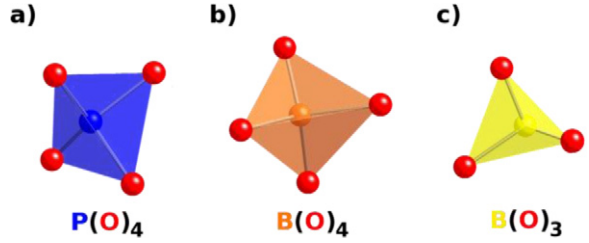

Figure 3. Basic structural units in $(Na_2O)_{0.35}[(P_2O_5)_{1-x}(B_2O_3)_x]_{0.65}$ glasses: from left to right, $P(O)_4$ tetrahedra, $B(O)_4$ tetrahedra and $B(O)_3$ planar/trigonal units.

shown in table 3. Following the same approach, the final configuration of the $x = 0.8$ model was used to prepare an initial configuration for the $x = 0.6$ glass model. This model consisted of 912 Na, 677 P, 1016 B and 3675 O atoms and the density listed in table 2.

All of the models constructed here were refined against the respective experimental $S(q)$ and $g(r)$ data until the latter were reproduced in the finest detail and the respective goodness-of-fit factors [11–13] reached values of a few per cent. As can be seen in figures 1 and 2, all initial model atomic configurations converged to structure models that reproduce the experimental XRD data both in reciprocal and real space very well. The models also have the correct stoichiometry and density of the glasses they represent. Important details for the $(Na_2O)_{0.35}[(P_2O_5)_{1-x}(B_2O_3)_x]_{0.65}$ structure glasses were revealed when the respective models were analyzed in terms of the type and relative abundance of glass structure building units, partial atomic distribution functions (shown in figure 4), partial structure functions (shown in figure 5) and distribution of bond angles (shown in figure 6). The analyses were performed with the help of the program ISAACS [21].

4. Discussion

The relative abundance of the structural building units in $(Na_2O)_{0.35}[(P_2O_5)_{1-x}(B_2O_3)_x]_{0.65}$ glasses and their connectivity, in terms of the number of bridging oxygen atoms and unlike first atomic neighbors, are shown in tables 4–7. The data presented in the tables are quantities extracted from 3D structure models that have been tested and refined against experimental data and not just reasonable assumptions invoked to explain particular experimental features. In this respect, the XRD/RMC approach employed here complements spectroscopy-based (e.g. Raman, IR, NMR) techniques which can identify the type and atomic fractions of the various structural units in glasses, but are less capable, except for the most sophisticated of NMR experiments, of determining the connectivity of these units in forming the continuous glass structure. In line with the findings of the preliminary analysis of the experimental RDF data, the information presented in tables 4–7 confirms that the glasses studied here are built of well defined $P(O)_4$, $B(O)_4$ and $B(O)_3$ structural units. Sketches of those structural units are shown in figure 3. There are only $P(O)_4$ tetrahedra in the glass with $x = 0$ (see table 4) and so the first peak in the experimental RDF data appears sharp and positioned at 1.52(2) Å (see figure 1). That peaks retains their position and sharpness throughout the whole series

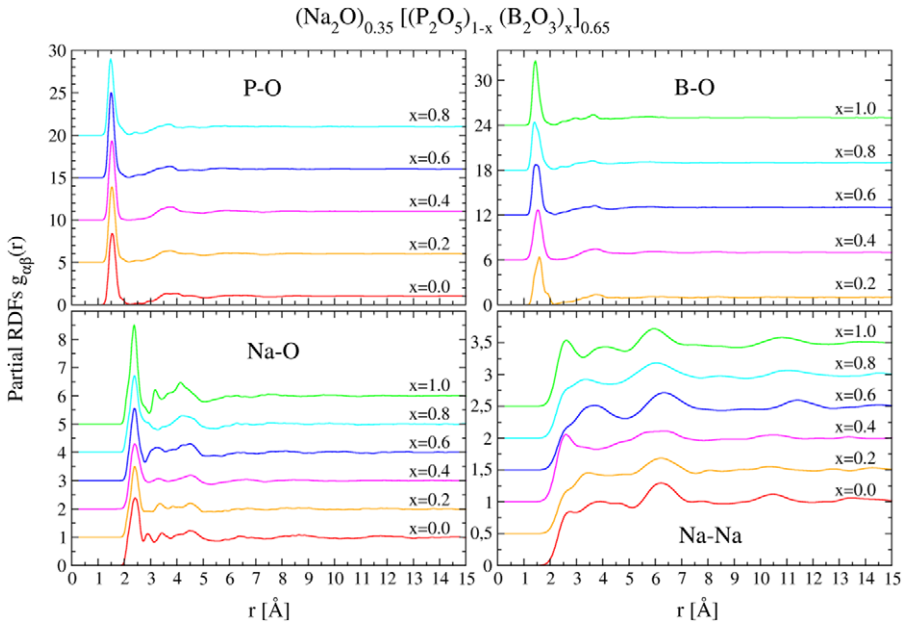

Figure 4. Atomic partial radial distribution functions for $(Na_2O)_{0.35}[(P_2O_5)_{1-x}(B_2O_3)_x]_{0.65}$ glasses: P–O partial distribution functions (top left), B–O partial distribution functions (top right), Na–O partial distribution functions (bottom left) and Na–Na partial distribution functions (bottom right). The data sets have been shifted up by a constant factor for clarity. Note that none of the partial atomic correlations show sharp features above approximately 10 Å, confirming the glass nature of the RMC models constructed in this work.

of glasses studied (see the P–O partial RDFs shown in figure 4) indicates that the boron-based structural units do not destroy the $P(O)_4$ tetrahedra but co-exist with them. This conclusion is confirmed by the O–P–O bond angle distribution (see figure 6) which appears to peak close to the tetrahedral angle of ∼109° for[6] all B-containing glasses studied here. When present in a relatively small amount (i.e. in glasses with $x = 0.2$ and 0.4) boron atoms also form well defined $B(O)_4$ tetrahedral units (see tables 5–7). As a result, the first peak in the B–O partial RDFs appears centered at about 1.5(2) Å (see figure 4). When present in a larger amount (i.e. in glasses with $x = 0.6$, 0.8 and 1.0), boron atoms form both $B(O)_4$ units and planar $B(O)_3$ units. The relative amount of the latter increases with x, reaching a maximum for $x = 1.0$ (see tables 5–7 and figure 7). That is why the first peak in the B–O partial RDFs for the glasses with a higher boron content is seen to become broader and shift to r values of 1.4 Å (see figure 4) which are typical for planar $B(O)_3$ units [10, 15]. Thus, the glasses with a higher boron content contain boron atoms in two distinct oxygen coordinations and local symmetry states. This is confirmed by the respective O–B–O bond angle distributions shown in figure 6. The O–B–O angles for four-fold coordinated boron atoms peak at the characteristic bond angles of $B(O)_4$ tetrahedra (∼109°), while those for three-fold coordinated boron atoms peak at an angle of ∼120° which is characteristic for planar $B–O_3$ triangular units.

[6] The type of glass modifier, Na in our case, the degree of connectivity, i.e. the number of bridging (BO) and non-bridging (NBO) oxygens, and the type of glass former first neighbor(s), that could be P and/or B in our case, are known to have a measurable effect on the O–P–O bond angles in $P(O)_4$ tetrahedra as discussed in [9]. For example, (BO)–P–(BO) bonds may appear close to ∼102° while (BO)–P–(NBO) to ∼116°. The fact that the the O–P–O bond angle distribution shown in figure 6(a) is not quite uniform and changes in shape with x reflects the complex evolution of the degree and type of connectivity of the $P(O)_4$ units (see table 4) in the glasses studied here.

Table 5. Relative abundance (in%) of B-based units (all coordinations) in $(Na_2O)_{0.35}[(P_2O_5)_{1-x}(B_2O_3)_x]_{0.65}$ glasses given in terms of $B^{(n)}$ and the related, but more local-structure specific, $B^{(n)}_{mP}$ polyhedra where n = number of bridging oxygens and $mP \trianglelefteq n$ = number of phosphorus atom neighbors (see footnote 5). Note the total number of $B^{(n)}$ units (bold) in each of the glasses is normalized to 100%. The same normalization applies to the $B^{(n)}_{mP}$ units (italic).

	x				
	0.2	0.4	0.6	0.8	1.0
$B^{(1)}$	**5.2**	**3.1**	**3.0**	**1.0**	**1.0**
$B^{(1)}_{0P}$		*1.0*	*2.0*	*1.0*	*1.0*
$B^{(1)}_{1P}$	*5.2*	*2.1*	*1.0*		
$B^{(2)}$	**42.9**	**29.0**	**19.6**	**11.6**	**12.1**
$B^{(2)}_{0P}$		*1.7*	*7.6*	*5.2*	12.1
$B^{(2)}_{1P}$	*3.4*	*7.8*	*9.1*	*5.4*	
$B^{(2)}_{2P}$	*39.5*	*19.5*	*2.9*	*1.0*	
$B^{(3)}$	**17.9**	**26.9**	**46.9**	**47.7**	**43.2**
$B^{(3)}_{0P}$		*1.4*	*9.6*	27.2	43.2
$B^{(3)}_{1P}$	*2.1*	*5.7*	*18.7*	16.9	
$B^{(3)}_{2P}$	*7.2*	*13.6*	*14.0*	3.6	
$B^{(3)}_{3P}$	*8.6*	*6.2*	*4.6*		
$B^{(4)}$	**34.0**	**41.0**	**30.5**	**39.7**	**43.7**
$B^{(4)}_{0P}$		*1.3*	*2.1*	*12.4*	*43.7*
$B^{(4)}_{1P}$		*3.8*	*8.2*	*17.5*	
$B^{(4)}_{2P}$	*3.4*	*9.0*	*9.9*	*7.6*	
$B^{(4)}_{3P}$	*8.6*	*13.6*	*8.1*	*2.2*	
$B^{(4)}_{4P}$	*22.0*	*13.3*	*2.2*		

Table 6. Relative abundance (in%) of tetrahedral (four-fold oxygen coordination) B-based units in $(Na_2O)_{0.35}[(P_2O_5)_{1-x}(B_2O_3)_x]_{0.65}$ glasses given in term of $B^{(n)}$ and the related, but more local-structure specific, $B^{(n)}_{mP}$ polyhedra where n = number of bridging oxygens and $mP \trianglelefteq n$ = number of phosphorus atom neighbors (see footnote 5). Note the total number of $B^{(n)}$ units (bold) in each of the glasses is normalized to 100%. The same normalization applies to the $B^{(n)}_{mP}$ units (italic).

	x				
	0.2	0.4	0.6	0.8	1.0
$B^{(1)}$	**5.8**	**2.5**	**1.2**	**1.0**	
$B^{(1)}_{0P}$			*1.2*	*1.0*	
$B^{(1)}_{1P}$	*5.8*	*2.5*			
$B^{(2)}$	**40.9**	**27.6**	**11.7**	**4.8**	**4.4**
$B^{(2)}_{0P}$		*1.8*	*3.1*	*2.1*	4.4
$B^{(2)}_{1P}$	*1.5*	*6.8*	*7.2*	*1.5*	
$B^{(2)}_{2P}$	*39.4*	*19.0*	*1.4*	*1.2*	
$B^{(3)}$	**16.9**	**26.2**	**42.3**	**18.0**	**15.6**
$B^{(3)}_{0P}$		*1.4*	*7.0*	*7.1*	15.6
$B^{(3)}_{1P}$	*2.3*	*6.1*	*17.7*	*8.4*	
$B^{(3)}_{2P}$	*8.1*	*14.0*	*14.4*	*2.5*	
$B^{(3)}_{3P}$	*6.6*	*4.7*	*3.2*		
$B^{(4)}$	**36.3**	**43.4**	**44.5**	**76.1**	**80.0**
$B^{(4)}_{0P}$		*1.4*	*3.2*	*24.7*	*80.0*
$B^{(4)}_{1P}$		*4.5*	*12.4*	*34.3*	
$B^{(4)}_{2P}$	*4.6*	*10.2*	*14.7*	*13.7*	
$B^{(4)}_{3P}$	*8.9*	*14.4*	*12.1*	*3.4*	
$B^{(4)}_{4P}$	*22.8*	*12.9*	*2.1*		

Table 7. Relative abundance (in%) of trigonal (three-fold oxygen coordination) B-based units in $(Na_2O)_{0.35}[(P_2O_5)_{1-x}(B_2O_3)_x]_{0.65}$ glasses given in terms of $B^{(n)}$ and the related, but more local-structure specific, $B^{(n)}_{mP}$ polyhedra where n = number of bridging oxygens and $mP \trianglelefteq n$ = number of connected phosphorus atom neighbors (see footnote 5). Note the total number of $B^{(n)}$ units (bold) in each of the glasses is normalized to 100%. The same normalization applies to the $B^{(n)}_{mP}$ units (italic).

	x				
	0.2	0.4	0.6	0.8	1.0
$B^{(1)}$	**17.9**	**10.2**	**5.6**	**2.2**	**1.5**
$B^{(1)}_{0P}$		*3.4*	*3.5*	*1.1*	1.5
$B^{(1)}_{1P}$	*17.9*	*6.8*	*2.1*	*1.1*	
$B^{(2)}$	**50.0**	**42.3**	**43.1**	**16.7**	**21.9**
$B^{(2)}_{0P}$		*1.7*	*16.9*	*8.6*	21.9
$B^{(2)}_{1P}$	*17.9*	*22.0*	*13.3*	*8.1*	
$B^{(2)}_{2P}$	*32.1*	*18.6*	*5.9*		
$B^{(3)}$	**30.1**	**47.8**	**58.3**	**80.7**	**76.6**
$B^{(3)}_{0P}$		*1.7*	*15.1*	*49.0*	76.6
$B^{(3)}_{1P}$	*3.6*	*10.2*	*21.6*	*26.0*	
$B^{(3)}_{2P}$	*7.1*	*15.6*	*14.2*	*5.7*	
$B^{(3)}_{3P}$	*21.4*	*20.3*	*7.4*		

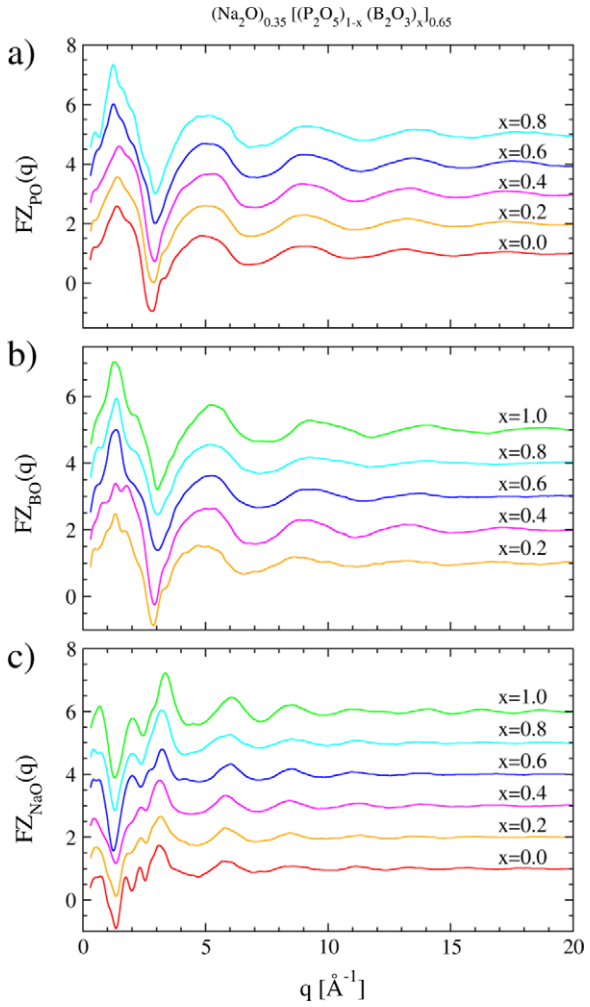

Figure 5. Partial structure functions (Faber–Ziman type) for $(Na_2O)_{0.35}[(P_2O_5)_{1-x}(B_2O_3)_x]_{0.65}$ glasses. The data sets have been shifted up by a constant factor for clarity. Note the complex behavior of all partial structure factors at low Q-values. This indicates that the first sharp diffraction peak(s) in the experimental $S(Q)$ data is(are) not due to a particular interatomic correlation/structural unit type but to structural features originating from the glass structure as a whole.

The distribution of Na atoms in the void space of the glass network does not seem to change much, remaining rather uniform with the changing P/B relative content. This is demonstrated by the similarity between the Na–O partial RDFs shown in figure 4. Also, Na atoms do not seem to cluster together since Na–Na partial RDFs are rather featureless for all x (see figure 4). Other studies on glasses of similar chemical composition have also concluded that Na atoms tend to distribute randomly inside the cavities of the glass network [22].

A careful look at the data in tables 4–7 allows to understand the evolution of the glass structure with changing relative P to B content. For $x = 0$ the glass structure is entirely made of $P(O)_4$ units. The majority of those units (68.6%) share two of their corners, resulting in the formation of long chains. For $x = 0.2$ the glass is made of both $P(O)_4$ and $B(O)_4$ units that are well mixed and coupled together, leading to an overall increase in the connectivity of the glass structure, i.e. in an

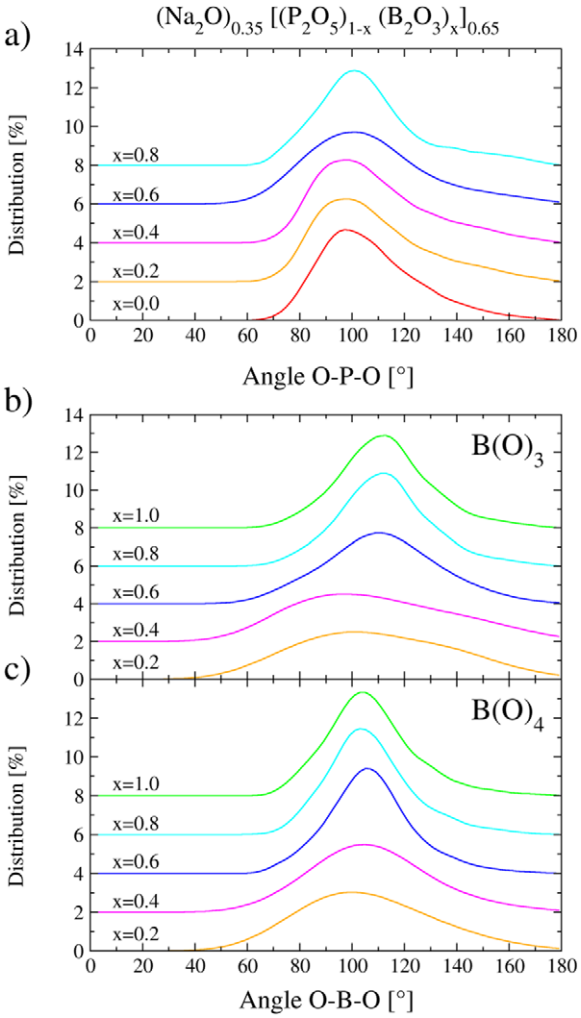

Figure 6. O–P–O and O–B–O bond angle distributions in $(Na_2O)_{0.35}[(P_2O_5)_{1-x}(B_2O_3)_x]_{0.65}$ glasses as revealed by the present studies. Two O–B–O distributions are shown: one for the boron atoms in tetrahedral and one for the boron atoms in planar trigonal coordination. They are seen to become narrower with increasing of B content, indicating that the respective $B(O)_4$ and $B(O)_3$ units become better defined (i.e. less deformed) when x approaches one. The O–P–O bond angle distribution is rather broad for all x, indicating that the $P(O)_4$ tetrahedra do not remain as well defined (see footnote 6) as the B–O units across the glass system studied. The higher level of 'rigidity' of B–O units reflects the fact that B–O bonds are stronger than P–O ones.

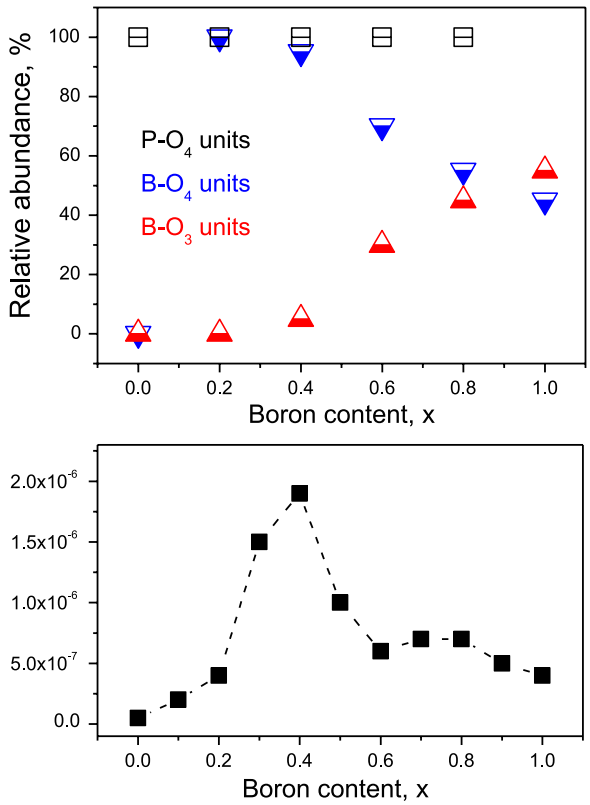

Figure 7. Relative abundance of the structural building units in $(Na_2O)_{0.35}[(P_2O_5)_{1-x}(B_2O_3)_x]_{0.65}$ glasses as revealed by the present study (top). Room temperature conductivity data (in S cm $^{-1}$) for $(Na_2O)_{0.35}[(P_2O_5)_{1-x}(B_2O_3)_x]_{0.65}$ [19]. The size of the symbols in the plot gives an idea of the accuracy (see footnote 5) of the respective data sets.

increase in the relative number of units having three and four bridging oxygen atoms. For the $x = 0.4$ glass, the majority of boron atoms still form $B(O)_4$ units but a small fraction of the boron atoms adopt $B(O)_3$ coordination as well (see figure 7). Yet the overall connectivity of the P- and B-based structural units remains quite high (see tables 4 and 5). The ratio of $B(O)_3$ to $B(O)_4$ units increases with x (see figure 7), and so the glasses with $x = 0.6$ and 0.8 show a complex structure of well-connected (i.e. containing two, three and four bridging oxygen atoms) $P(O)_4$, $B(O)_4$ and $B(O)_3$ units. In the $x = 1$ glass only B-based (i.e. $B(O)_4$ and $B(O)_3$) units are present and those units again are quite well connected (see table 5).

The richness of structural units and the relatively high level of connectivity in the atomic-scale structure of the glasses studied here is well demonstrated in figure 8, where snapshots of the RMC constructed 3D models are shown. Now the evolution of the low-Q features/peaks in the experimental $S(Q)$ data (see figure 1), i.e. the evolution of the medium-range order in $(Na_2O)_{0.35}[(P_2O_5)_{1-x}(B_2O_3)_x]_{0.65}$ glasses, is easier to understand. It reflects the gradual evolution of the glass structure from being an assembly of relatively long chains of $P(O)_4$ tetrahedra (for $x = 0$) to an assembly of $P(O)_4$, $B(O)_4$ and $B(O)_3$ macro (i.e. well connected between each other) units (for $x > 0$).

From the point of view of Na atoms this evolution will result in them having first oxygen neighbors that, although not changing in number, gradually change the type of structural units they belong to with changing x. In particular, in the $x = 0$ glass all O atoms share charge with P atoms and participate in $P(O)_4$ units. In the boron and phosphorus containing glasses some O atoms will share charge with only P, some with only B atoms and others—with both P and B atoms (see tables 4–7). Furthermore, the way B atoms and oxygen share charge is different in the case of $B(O)_4$ and $B(O)_3$ units. All this will result in Na atoms facing oxygen neighbors with quite different negative charge distributions, i.e. facing quite different conductivity activation local energy barriers when x

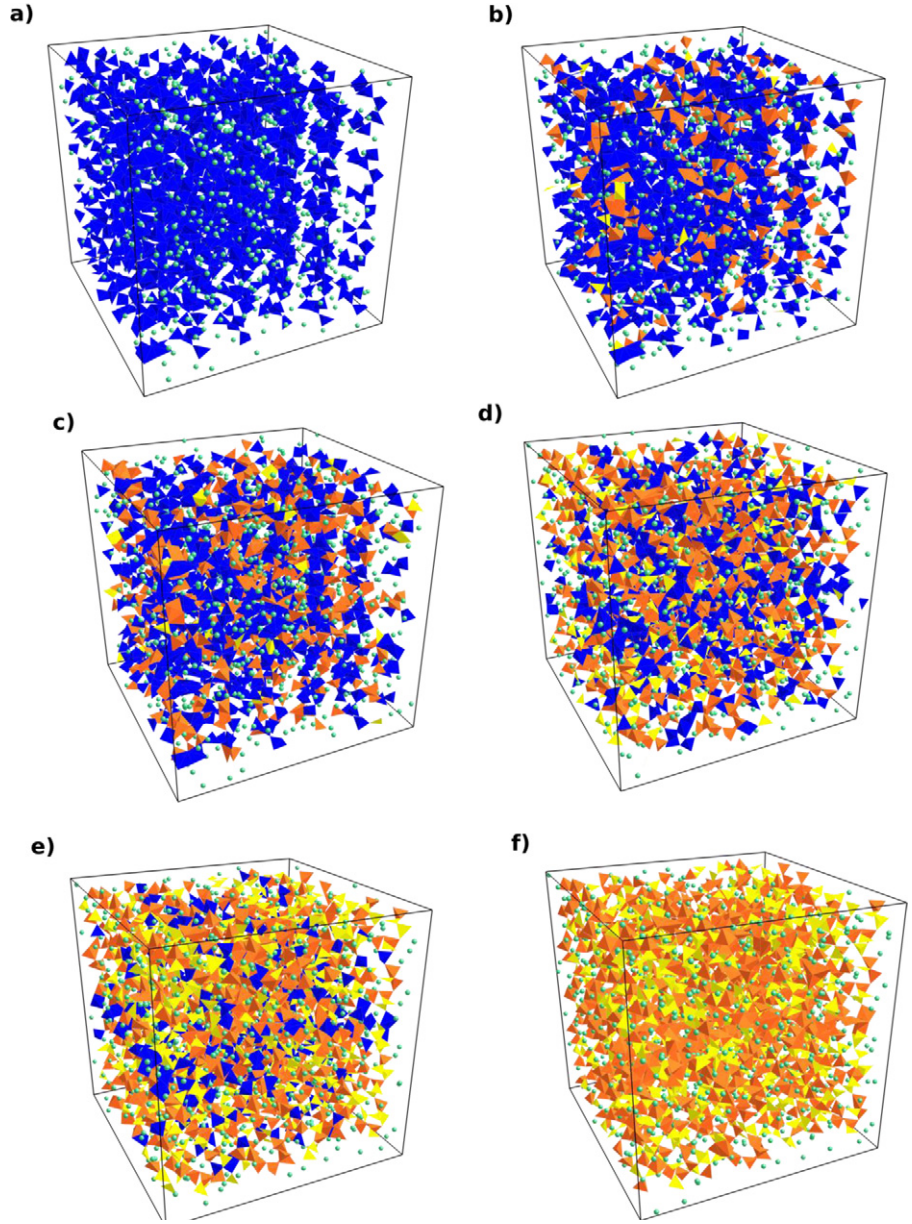

Figure 8. RMC constructed three-dimensional models for $(Na_2O)_{0.35}[(P_2O_5)_{1-x}(B_2O_3)_x]_{0.65}$ glasses: (a) $x = 0.0$, (b) $x = 0.2$, (c) $x = 0.4$, (d) $x = 0.6$, (e) $x = 0.8$ and (f) $x = 1.0$. Sodium atoms (dots) appear in green (light gray) and the coordination polyhedra are highlighted as follows: tetrahedral $P(O)_4$ in blue (black), tetrahedral $B(O)_4$ in orange (dark gray) and trigonal $B(O)_3$ in yellow (light gray).

changes from zero to one. And when this is the case strong nonlinearity in the Na ion conductivity can occur as discussed in [23].

Next logical step along this line would be to assign values for the energy barriers carried by the structurally different oxygen atoms/oxygen polyhedra in $(Na_2O)_{0.35}[(P_2O_5)_{1-x}(B_2O_3)_x]_{0.65}$ glasses, map those onto the RMC structure models and study the conductivity behavior of Na atoms inside thus constructed 3D energy landscape. In this way, the structure–conductivity property relationship in $(Na_2O)_{0.35}[(P_2O_5)_{1-x}(B_2O_3)_x]_{0.65}$ glasses could be better assessed and therefore better understood. Unfortunately no precise values for the energy barriers/interactions between the conductive alkali ions and the structural units in glasses are known. Deriving good estimates for those values and using them as described above is work in progress that will be reported separately. What can be done within the scope of the present study is to look for a correlation between the composition dependence of the various structural units in $(Na_2O)_{0.35}[(P_2O_5)_{1-x}(B_2O_3)_x]_{0.65}$ glasses and the observed nonlinearity of Na conductivity in the manner suggested in [2].

As can be seen in figure 7, the appearance of $B(O)_4$ units and the decay of their relative concentration at the expense of $B(O)_3$ units nicely correlates with the jump and fall off of Na conductivity, respectively. The result implies that, given a constant Na content, the interplay between $B(O)_4$ and $B(O)_3$ units drives the nonlinear behavior of the conductivity of Na ions inside sodium borophosphate glasses.

5. Conclusion

High-energy XRD has been used to study $(Na_2O)_{0.35}[(P_2O_5)_{1-x}(B_2O_3)_x]_{0.65}$ glasses with $x = 0$, 0.2, 0.4, 0.6, 0.8 and 1.0. The XRD data have been used as a basis for constrained RMC simulations of the structure of these glasses. Experiments and simulations show that the glasses have a complex structure that evolves from chains of $P(O)_4$ tetrahedra for $x = 0$ to an assembly of well-connected $P(O)_4$, $B(O)_4$ and $B(O)_3$ units for $x > 0$. The new structural information opens up the road to a detailed exploration of the origin of the MGFE effect observed in this glass system.

Acknowledgments

Work on the project was supported by NSF DMR grant 0710564. APS is supported by DOE under contract number DE-AC02-06CH11357.

References

[1] Zielniok D, Cramer C and Eckert H 2007 *Chem. Mater.* **19** 3162–70
[2] Zielniok D, Eckert H and Cramer C 2008 *Phys. Rev. Lett.* **100** 035901
[3] Kim Y, Saienga J and Martin S W 2006 *J. Phys. Chem.* B **110** 16318–25
[4] Le Messurier D, Petkov V, Martin S W, Youngsik K and Ren Y 2009 *J. Non-Cryst. Solids* **355** 430–7
[5] Petkov V, Qadir D and Shastri S 2004 *Solid State Commun.* **129** 239–43
[6] Petkov V, Billinge S J L, Shastri S and Himmel B 2000 *Phys. Rev. Lett.* **85** 3436–9
[7] Wagner C N J 1978 *J. Non-Cryst. Solids* **31** 1
[8] Petkov V 1989 *J. Appl. Crystallogr.* **22** 387–9 RAD is available free at http://www.phy.cmich.edu/people/petkov/software.html
[9] Hoppe U, Walter G, Kranold R and Stachel D 2000 *J. Non-Cryst. Solids* **263** 29–47
[10] Fabian M, Svab E, Proffen Th and Veress E 2010 *J. Non-Cryst. Solids* **356** 441–6
[11] McGreevy R L and Pusztai L 1988 *Mol. Simul.* **1** 359–67
[12] Dove M T 2002 *EMU Notes Mineral.* **4** 59–82
[13] Gereben O, Jóvári P, Temleitner L and Pusztai L 2007 *J. Optoelectron. Adv. Mater.* **9** 3021–7
[14] McAdam A, Jost K H and Beagley B 1968 *Acta Crystallogr.* B **24** 1621–2
[15] Wright A C, Shaw J L, Sinclair R N, Vedishcheva N M, Shakhmatkin B A and Scales C R 2004 *J. Non-Cryst. Solids* **345** 24–33
[16] Muller C R, Kathriarachchi V, Schuch P, Mass P and Petkov V 2010 *Phys. Chem. Chem. Phys.* **12** 10444–51
[17] Petkov V and Le Messurier D 2010 *J. Phys.: Condens. Matter* **22** 115402
[18] Christensen R, Byer J, Kaufmann T and Martin S W 2009 *Phys. Chem. Glasses—Europ. J. Glass Sci. Technol.* B **50** 237–42
[19] Krogh-Moe J 1974 *Acta Crystallogr.* B **30** 578–82
[20] Sayle D C, Mangili B C, Price D W and Sayle T X 2010 *Phys. Chem. Chem. Phys.* **12** 8584–96
[21] Le Roux S and Petkov V 2010 *J. Appl. Crystallogr.* **43** 181–5 ISAACS is available free at http://www.phy.cmich.edu/people/petkov/isaacs/
[22] Alam T M, McLaughlin J, Click C C, Conzone S, Brow R K, Boyle T J and Zwanziger J W 2006 *J. Phys. Chem.* B **104** 1464–72
[23] Schuch M, Muller Ch R, Maass P and Martin S W 2009 *Phys. Rev. Lett.* **102** 145902